Proceedings of GT2006
ASME Turbo Expo 2006: Power for Land, Sea and Air
May 8-11, 2006, Barcelona, Spain

GT2006-90742

Simulation of Mist Film Cooling at Gas Turbine Operating Conditions

Ting Wang and Xianchang Li
Energy Conversion & Conservation Center
University of New Orleans
New Orleans, LA 70148-2220

ABSTRACT

Air film cooling has been successfully used to cool gas turbine hot sections for the last half century. A promising technology is proposed to enhance air film cooling with water mist injection. Numerical simulations have shown that injecting a small amount of water droplets into the cooling air improves film-cooling performance significantly. However, previous studies were conducted at conditions of low Reynolds number, temperature, and pressure to allow comparisons with experimental data. As a continuous effort to develop a realistic mist film cooling scheme, this paper focuses on simulating mist film cooling under typical gas turbine operating conditions of high temperature and pressure. The mainstream flow is at 15 atm with a temperature of 1561K. Both 2-D and 3-D cases are considered with different hole geometries on a flat surface, including a 2-D slot, a simple round hole, a compound-angle hole, and fan-shaped holes. The results show that 10%-20% mist (based on the coolant mass flow rate) achieves 5%-10% cooling enhancement and provides an additional 30-68K adiabatic wall temperature reduction. Uniform droplets of 5 to 20 μm are used. The droplet trajectories indicate the droplets tend to move away from the wall, which results in a lower cooling enhancement than under low pressure and temperature conditions. The commercial software Fluent (v. 6.2.16) is adopted in this study, and the standard k-ε model with enhanced wall treatment is adopted as the turbulence model.

Nomenclature

b	slot width (m)
C	concentration (kg/m^3)
c_p	specific heat (J/kg-K)
D	mass diffusion coefficient (m^2/s)
d	diameter (m)
F	force (N)
GT	gas turbine
H_{12}	Boundary layer shape factor, δ_1/δ_2
k	turbulence kinetic energy (m^2/s^2)
k_c	mass transfer coefficient (m/s)
h	convective heat transfer coefficient (W/m^2-K)
h_{fg}	latent heat (J/kg)
M	blowing ratio, $(\rho u)_c/(\rho u)_g$
m	mass (kg)
P	pressure (N/m^2)
Pr	Prandtl number, ν/α
Re_l	main flow Reynolds number based on chord length, ul/ν
Re_d	jet Reynolds number based on slot width or cooling hole diameter, ub/ν or ud/ν.
S	source term
T	temperature (K, ^{o}F)
t	time (s)
u	streamwise velocity component (m/s)
v	spanwise velocity component (m/s)
x, y, z	coordinates

Greek

α	thermal diffusivity (m^2/s)
ε	turbulence dissipation rate (m^2/s^3)
$\delta, \delta_1, \delta_2$	boundary layer, displacement, momentum thickness
η	adiabatic film cooling effectiveness, $(T_g-T_{aw})/(T_g-T_c)$
λ	heat conductivity (W/m-K)
μ	dynamic viscosity (kg/m-s)
ν	kinematic viscosity (m^2/s)
ρ	density (kg/m^3)
τ	stress tensor (kg/m-s^2)

Subscript

aw	adiabatic wall
c	coolant or jet flow
g	hot gas/air
p	particle or droplet
0	values for air film cooling without mist
∞	far away from droplets

INTRODUCTION

The gas turbine thermal efficiency can be generally increased by using high turbine inlet temperature, which makes the cooling of gas turbine hot components such as combustor liners, combustor transition pieces, turbine vanes (nozzles) and blades (buckets) a critical task. Different cooling technologies including internal and air film cooling have been successfully used to cool these hot sections for the last half century. To continuously increase the thermal efficiency and lower the fuel cost, the inlet gas temperature will be further raised. The load to cool hot sections will increase accordingly. Consequently,

significant efforts of both numerical simulation and experimental tests have been made to improve film-cooling performance. For example, studies have been conducted to investigate the optimal geometries of coolant injection including injection angle of forward inclination (Jia et al. [1], Bell et al. [2], Brittingham and Leylek [3] and Taslim and Khanicheh [4]) and blowing ratio (Jia et al. [1], Kwak and Han [5], and Mayhew et al. [6]). These parameters are essential to determine the jet separation and flow recirculation near the injection hole and flow mixing in the far downstream.

Bell et al. [2], Brittingham and Leylek [3] and Wang et al. [7] investigated the cooling performance of the shaped holes with various configurations including lateral or forward diffusion, and compound-angle holes with forward diffusion. In most cases, the simple forward hole results in a strong secondary flow (the flow perpendicular to the mainstream), which brings the hot gas to the wall and degrades the cooling effectiveness. The shaped holes perform better by reducing or redirecting the jet momentum. The performance of film cooling with different holes varies by 30~50% subject to geometric and flow conditions.

Flow conditions, such as inlet turbulence intensity, mixing in the coolant supply chamber, and inlet velocity profiles, have also been investigated by many researchers. For example, low inlet turbulence intensity keeps the coolant close to the wall when the blowing ratio is low, while high inlet turbulence intensity helps bring the coolant back towards the wall when the blowing ratio is high (Mayhew et al. [6]). The effect of flow conditions in the supply chamber on film cooling was studied by Brittingham and Leylek [3], and Adami et al. [8], etc. Theoretically, the flow pattern in the supply plenum would affect the coolant velocity profile and turbulence intensity at the jet discharge.

In experiments, both infrared image and transient liquid crystal schemes have been commonly employed to obtain the surface temperature and cooling effectiveness [9-10]. When computational simulation is conducted, selections of turbulent models may affect the results. The effects of turbulence modeling on film cooling simulations have been investigated by a number of researchers. For example, the V2F k-ε turbulence model was employed by Jia et al. [1], the standard k-ε model by Brittingham and Leylek [3], and k-ω model by Heidmann et al. [11]. Recently, Tyagi and Acharya [12] employed a large eddy simulation (LES) scheme to investigate the detailed coherent flow structures of film cooling. Numerical simulation can provide ideal boundary conditions but may fail to accurately predict the flow separation and correct physics. Nevertheless, most published work did not employ the real gas turbine operating conditions at high temperature and pressure.

Studies of other specific parameters on gas turbine film cooling have also been conducted, such as the cooling of trailing edge cut-back [13], the leading edge without rotation [14], and the effect of surface roughness on film cooling [15].

While the net benefit from improving traditional cooling methods seems to be marginally incremental, and the working gas temperature is continuously elevated to improve the thermal efficiency of gas turbines, new cooling techniques are needed to surpass the current limits. A promising technology is to enhance film cooling with mist (small water droplets) injection. The most important feature of mist cooling is its "distributed cooling" characteristics. Each droplet acts as a cooling sink, and it flies a distance before it completely vaporizes. The reduced temperature near the surface due to droplet evaporation near the wall plays a major role in protecting the surface from the hot gas. Direct contacts between water droplets and the wall further take the thermal energy away at a fast pace, which significantly enhance cooling effectiveness. The reduced bulk temperature due to water droplet evaporation in the film coolant stream increases temperature gradient and results in high heat diffusion and convection between the coolant and the wall. The augmented mixing induced by droplet-air interactions and increased specific heat also supplement the cooling enhancement. Furthermore, the continuous evaporation of droplets can last farther into the downstream region where single-phase air film cooling becomes less effective. Based on the aforementioned heat transfer mechanisms, mist can be used in gas turbine systems in different ways, including gas turbine inlet air fog cooling [16], overspray cooling through wet compression in the compressor [17], and airfoils (vanes and blades) internal cooling [18-21].

Recently, Li and Wang [22] conducted the first numerical simulations of air/mist film cooling. They showed that injecting a small amount of droplets (2% of the coolant flow rate) could enhance the cooling effectiveness about 30% ~ 50%. The cooling enhancement takes place more strongly in the downstream region, where the single-phase film cooling becomes less powerful. Three different holes were used in their study, including a 2-D slot, a round hole, and a fan-shaped diffusion hole. They performed a comprehensive study on the effect of flue gas temperature, blowing angle, blowing ratio, mist injection rate, and droplet size on the cooling effectiveness. Analysis on droplet history (trajectory and size) was undertaken to interpret the mechanisms of droplet dynamics.

Following [22], Li and Wang [23] continued a more fundamental study on investigating the effect of various models on the computational results including the turbulence models, dispersed-phase modeling, different forces models (Saffman, thermophoresis, and Brownian), trajectory tracking model, near-wall grid arrangement, and mist injection scheme. The effects of flow inlet boundary conditions (with/without the air supply plenum), inlet turbulence intensity, and the near-wall grid density on simulation results were also investigated. Using a 2-D slot film cooling simulation with a fixed blowing angle and blowing ratio, they showed that injecting mist of 2% coolant mass flow rate can increase the adiabatic cooling effectiveness about 45%. The RNG k-ε model, RSM and the standard k-ε turbulence model with the enhanced wall treatment produce consistent and reasonable results, while the turbulence dispersion has a significant effect on mist film cooling through the stochastic trajectory calculation. The thermophoretic force slightly increases the cooling effectiveness, but the effect of Brownian force and Saffman lift is imperceptible. The cooling performance is affected negatively by the plenum, which alters the velocity profile and turbulence intensity at the jet discharge plane.

The studies in [22-23] were conducted at conditions of low Reynolds number, temperature, and pressure. Actually, most other studies discussed above were also conducted at low Reynolds number, temperature, and pressure conditions. As a continuous effort to develop a realistic mist film cooling scheme, this paper focuses on simulating mist film cooling over a flat surface under gas turbine operating conditions of high temperature and pressure. Both 2-D and 3-D cases are considered with different jet geometries, including a 2-D slot, a simple hole, a fan-shaped hole, and a compound hole. The results of this paper can serve as a reference for future experimental validation and technical implementation to real gas turbine applications.

NUMERICAL MODEL

Recognizing that the experiments at gas turbine operating conditions are difficult and expensive to be conducted, especially for the study with mist injection, this study employs a numerical simulation to provide a preliminary examination of mist film cooling performance under elevated gas turbine operating conditions. A

feasible method to simulate the film cooling with mist injection is to consider the droplets as a discrete phase since the volume fraction of the liquid is usually small (less than 1%). The trajectory of droplets is tracked by using a Lagrangian method. By calculating heat and mass transfer between droplets and airflow, the droplet evaporation and size can be known. Correspondingly, the effect of droplets on the airflow is incorporated into the equation of mass and energy conservation as a source term. This multiphase computational scheme has been used to solve many different problems [24-26].

The following are the governing equations of mass, momentum, energy and species, which are based on time-averaged steady state conditions.

$$\frac{\partial}{\partial x_i}\left(\rho u_i\right) = S_m \tag{1}$$

$$\frac{\partial}{\partial x_i}\left(\rho u_i u_j\right) = \rho \bar{g}_j - \frac{\partial P}{\partial x_j} + \frac{\partial}{\partial x_i}\left(\tau_{ij} - \rho\overline{u'_i u'_j}\right) + F_j \tag{2}$$

$$\frac{\partial}{\partial x_i}\left(\rho c_p u_i T\right) = \frac{\partial}{\partial x_i}\left(\lambda \frac{\partial T}{\partial x_i} - \rho c_p \overline{u'_i T'}\right) + \mu\Phi + S_h \tag{3}$$

$$\frac{\partial}{\partial x_i}\left(\rho u_i C_j\right) = \frac{\partial}{\partial x_i}\left(\rho D_j \frac{\partial C_j}{\partial x_i} - \rho\overline{u'_i C'_j}\right) + S_j \tag{4}$$

where τ_{ij} is the symmetric stress tensor. The source terms (S_m, F_j and S_h) are used to include the contributions from the dispersed phase. $\mu\Phi$ is the viscous dissipation and λ is the heat conductivity. C_j is the mass fraction of the species (j) in the mixture, and S_j is the source term for this species. D_j is the diffusion coefficient. Three species (oxygen, nitrogen and water vapor) need to be simulated in mist film cooling flow.

The terms of $\rho\overline{u'_i u'_j}$, $\rho c_p\overline{u'_i T'}$, and $\rho\overline{u'_i C'_j}$ in the equations above represent the Reynolds stresses, turbulent heat fluxes, and turbulent concentration (or mass) fluxes, which should be modeled properly for a turbulent flow as seen in the film cooling of gas turbines. More detailed turbulence models and the effect on the simulation of film cooling with mist can be found in [22-23]. In this study, the standard k-ε model is used with the enhanced near-wall treatment. The equations for the turbulent kinetic energy (k) and its dissipation rate (ε) are:

$$\frac{\partial}{\partial x_i}\left(\rho u_i k\right) = \frac{\partial}{\partial x_i}\left[\left(\mu + \frac{\mu_t}{\sigma_k}\right)\frac{\partial k}{\partial x_i}\right] + G_k - \rho\varepsilon . \tag{5}$$

$$\frac{\partial}{\partial x_i}\left(\rho u_i \varepsilon\right) = \frac{\partial}{\partial x_i}\left[\left(\mu + \frac{\mu_t}{\sigma_\varepsilon}\right)\frac{\partial \varepsilon}{\partial x_i}\right] + C_{1\varepsilon}G_k\frac{\varepsilon}{k} - C_{2\varepsilon}\rho\frac{\varepsilon^2}{k} . \tag{6}$$

The term G_k is the generation of turbulence kinetic energy due to the mean velocity gradients. The turbulent viscosity, μ_t, is calculated from the equation

$$\mu_t = \rho C_\mu \frac{k^2}{\varepsilon} \tag{7}$$

and the effective heat conductivity (λ_{eff}) and the effective diffusion coefficient are calculated by the following two equations, respectively.

$$\lambda_{eff} = \lambda + c_p\mu_t / Pr_t , \tag{8}$$

$$D_{eff} = D + \mu_t / Sc_t . \tag{9}$$

The constants $C_{1\varepsilon}$, $C_{2\varepsilon}$, C_μ, σ_k, and σ_ε used are: $C_{1\varepsilon} = 1.44$, $C_{2\varepsilon} = 1.92$, $C_\mu = 0.09$, $\sigma_k = 1.0$, $\sigma_\varepsilon = 1.3$ [27]. The turbulence Prandtl number, Pr_t, is set to 0.85, and the turbulence Schmidt number, Sc_t, is set to 0.7.

For the near wall region, the enhanced wall treatment is used, in which the standard two-layer model is combined with wall functions. To apply the two-layer approach, the computational domain is separated into a viscosity-affected region and a fully-turbulent region by defining a turbulent Reynolds number, Re_y, which is based on the distance from the wall.

$$Re_y = yk^{1/2} / \nu \tag{10}$$

where k is the turbulence kinetic energy and y is the distance from the wall. The flow is assumed in the fully turbulent region if $Re_y > 200$, and the k-ε model is used. Otherwise, the flow is in the viscosity-affected region, and the one-equation model of Wolfstein [28] is used. The turbulent viscosities calculated from the two regions are blended with a blending function (θ) to make the transition smooth.

$$\mu_{t,enhanced} = \theta\mu_t + (1-\theta)\mu_{t,l} \tag{11}$$

where μ_t is the viscosity from the k-ε model of high Reynolds number, and $\mu_{t,l}$ is the viscosity from the near-wall one-equation model. The blending function is defined so it is 0 at the wall and 1 in the fully-turbulent region. The wall functions are also enhanced by blending linear (laminar) and logarithmic (turbulent) laws-of-the-wall to make the applicability throughout the entire near-wall region.

To track the trajectory of droplets, the hydrodynamic drag, gravity and forces such as the "virtual mass" force, thermophoretic force, Brownian force, and Saffman's lift force, etc. are combined to accelerate the droplet. The energy equation for any individual droplet can be given as the following equation.

$$m_p c_p \frac{dT}{dt} = \pi d^2 h(T_\infty - T) + \frac{dm_p}{dt} h_{fg} \tag{12}$$

where h_{fg} is the latent heat. The convective heat transfer coefficient (h) can be obtained with an empirical correlation [29-30]

The mass change rate or vaporization rate in Eq. (12) is governed by concentration difference between droplet surface and the air stream,

$$-\frac{dm_p}{dt} = \pi d^2 k_c (C_s - C_\infty) \tag{13}$$

where k_c is the mass transfer coefficient, and C_s is the vapor concentration at the droplet surface, which is evaluated by assuming the flow over the surface is saturated. C_∞ is the vapor concentration of the bulk flow, obtained by solving the transport equations. When the droplet temperature reaches the boiling point, the following equation can be used to evaluate its evaporation rate [31]:

$$-\frac{dm_p}{dt} = \pi d^2\left(\frac{\lambda}{d}\right)(2.0 + 0.46Re_d^{0.5})\ln\left(1 + c_p(T_\infty - T)/h_{fg}\right)/c_p \tag{14}$$

where λ is the gas/air heat conductivity, and c_p is the specific heat of the bulk flow. Again, more details are documented in [22-23] for the model of discrete phase.

Stochastic method [32] is used to consider turbulence dispersion effect on droplets tracking. The droplet trajectories are calculated with the instantaneous flow velocity ($\bar{u} + u'$), and the velocity fluctuations are then given as:

$$u' = \varsigma\left(\overline{u'^2}\right)^{0.5} = \varsigma(2k/3)^{0.5} \tag{15}$$

where ζ is a normally distributed random number. This velocity will apply during the characteristic lifetime of the eddy (t_e), a time scale calculated from the turbulence kinetic energy and dissipation rate. After this time period, the instantaneous velocity will be updated with a new ζ value until a full trajectory is obtained.

Injection Configurations

Different injection holes are considered in this study, including a simple round hole, a fan-shaped hole, and a compound-angle hole. The forward angle is 35°, and the lateral diffusive angle is 14°. The inclination angle of the compound hole in the direction perpendicular to the mainstream is 30°. The initial diameter of the injection hole is 1 mm for all the 3 cases. The computational domain is 40d in the mainstream direction and 3d in the spanwise direction. The domain has a height of 10d. To study and compare the fundamental phenomena of mist film cooling, a 2-D slot is also used in this study, and the width of the slot is 1 mm. Figure 1 shows the injection configuration and the computational domain.

Boundary Conditions and Operating Parameters

As mentioned earlier, the focus of this study is on mist film cooling at gas turbine operating conditions, which means high velocity, temperature, heat flux, and pressure. The GT operating condition adopted in this study represents a general condition in F-frame type GT without trying to match the specific condition of any brand name or model. The main airflow (dry air) and the coolant air (saturated) are at 15 atm. The main flow has a uniform velocity of 128 m/s and a temperature of 1561 K (2350°F). Based on a chord length of 20 cm, these parameters give a Reynolds number approximately of 1.5 million (1.5×10^6). The jet flow is assumed at 644 K (700°F). To give a blowing ratio of 2, the jet velocity is assigned to 106 m/s. The blowing ratio (M) is defined as $M=(\rho u)_c/(\rho u)_g$. Note that these settings are only one possible case in the real gas turbine applications. The turbulent intensity of both the mainstream inlet and coolant flow inlet is 1% for most of the cases. Turbulence intensities of 5% and 10% are assigned to the mainstream later to examine the effect of FSTI (free-stream turbulence intensity) on film cooling performance. Periodic boundary condition is assigned in the spanwise direction for the compound-angle hole case, while symmetric boundary condition is used for other cases. All other walls are adiabatic and have a non-slip velocity boundary condition. The boundary condition at the domain outlet (x/d=30) is assigned as constant pressure at 15 atm.

Uniform droplet size is given as 5, 10 or 20 μm. Non-uniform droplets are assumed to perform as a combination of droplet with different uniform sizes. This assumption is based on the results found in [33], which showed that the effect of non-uniform particle size is bounded by the uniform droplet sizes between larger and smaller droplets. The mass ratio of mist over coolant flow ranges from 10 to 20%, considering that high temperature difference in the real application need more mist evaporation to achieve high cooling effectiveness. In the previous study with low pressure and temperature conditions, the injection amount of mist is only 2% of the coolant flow. The droplet initial temperature is 472K, which is the water saturation temperature at 15 atm.

Mist is injected uniformly from a surface perpendicular to the jet hole axis and close to the jet inlet. The total trajectories traced are about 3000. The boundary condition of droplets at walls is assigned as "reflect", which means the droplets elastically rebound off once reaching the wall. To examine the importance of droplets at the walls, another boundary condition "trap", which means "adhere to the wall and evaporate completely," is also considered. The real case will be bounded between these two cases. At the outlet, the droplets just simply flee/escape from the computational domain.

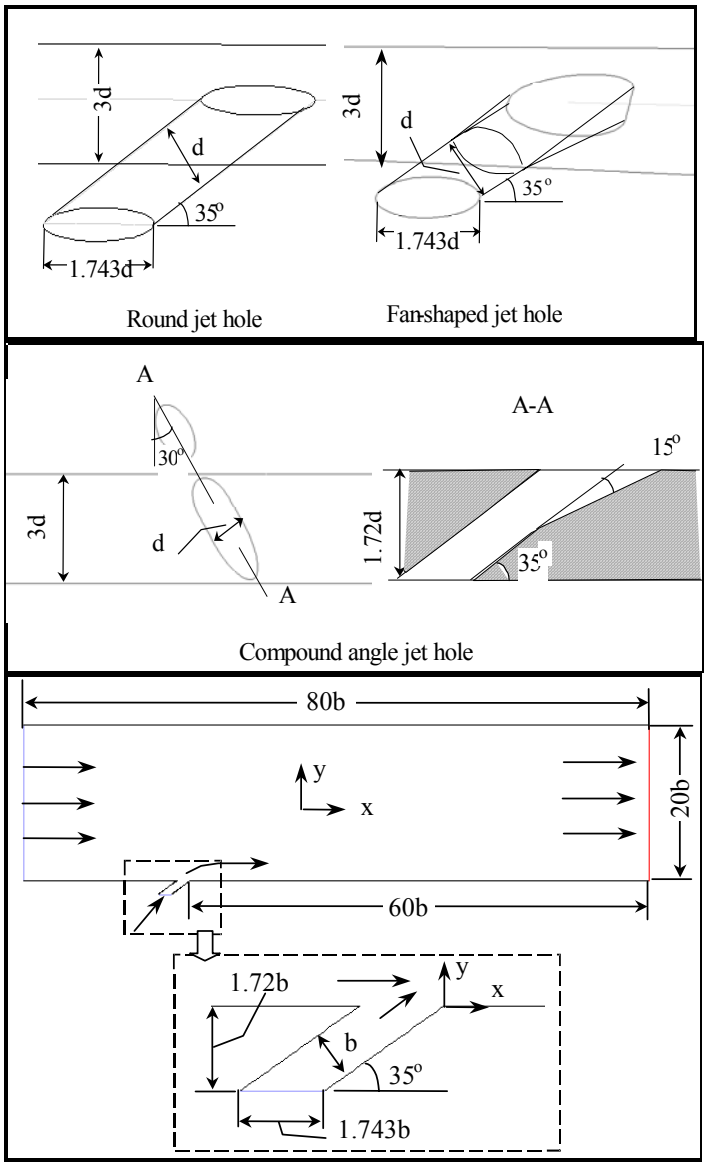

Figure 1 Computational domain and film hole configurations

Table 1 gives the comparison of air and water properties between low and high pressures and temperatures. At gas turbine operating conditions, air density changes significantly from the low temperature and pressure condition. In general, the dynamic viscosity does not significantly change with pressure but only with temperature. When the temperature increases from 400K to 1500 K, the dynamic viscosity increases about 2.4 times (55.7/23.0). The kinematic viscosity is related to the pressure through the density.

Table 1 Air and water (liquid) properties at different conditions

Air		400K 1 atm *	1500 K 15 atm **
	Density (kg/m^3)	0.871	3.483
	Specific heat (J/kg-K)	1014	1230
	Heat conductivity (W/m-K)	0.0338	0.1
	Dynamic viscosity × 10^6 (kg/m-s)	23.0	55.7
	Kinematic viscosity × 10^6 (m^2/s)	26.4	16.0
Water		1 atm	15 atm
	Saturation temperature (K)	373	472
	Specific heat (J/kg-K)	4180	4490
	Density (kg/m^3)	998	866
	Latent heat (kJ/kg)	1950	2260

* Nominal conditions in previous studies [22-23]
** Nominal conditions in the present study

Meshing and Numerical Procedure

Unstructured grids are applied to the jet holes and a small volume in the main domain close to the jet outlet. Structured but nonuniform grids are used for the rest of domain. There are 360,000 cells for the round-hole case and 296,000 cells for the fan-shaped hole case. Compound-angle hole case has 290,000 cells. Figure 2 shows the grids of the jet wall as well as the adjacent surface. Tetrahedron elements are generated for the jet hole and the region close to the jet. Other part of the domain is meshed with hexahedron elements. There are more grids close to the jet hole and wall to capture the important characteristics of film cooling flow. For the 2-D slot case, near-wall grid is "adapted" to examine the grid independence. Adaptation refines the grid in both streamwise and spanwise directions. The refined grid along the wall region reduces the y+ and y*. More detailed discussion and investigation of near-wall mesh effect on mist film cooling is referred to the previous study [23].

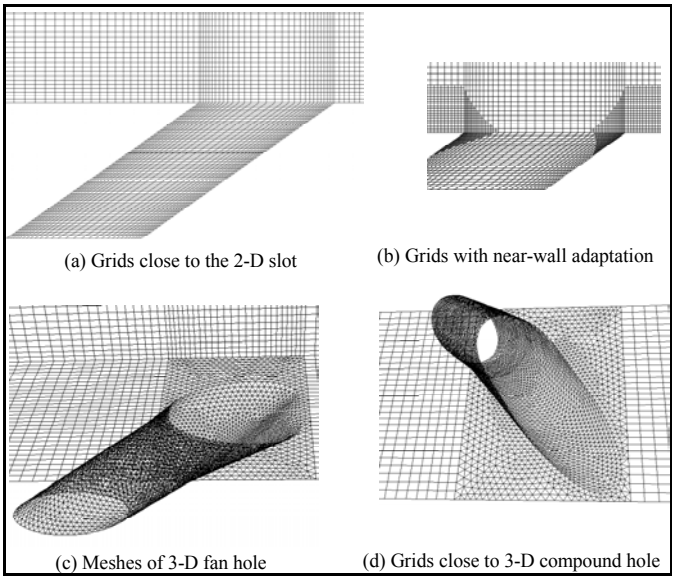

Figure 2 Meshes

The commercial software package Fluent (v. 6.2.16) from Fluent, Inc. is adopted in this study. Fluent employs a finite-volume method with second order upwind scheme for spatial discretization of the convective terms and species. Iteration proceeds alternatively between the continuous and the discrete phases. Ten iterations in the continuous phase are conducted between two iterations in the discrete phase. Converged results are obtained after the specified residuals are met. A converged result renders mass residual of 10^{-4}, energy residual of 10^{-6}, and momentum and turbulence kinetic energy residuals of 10^{-5}. These residuals are the summation of the imbalance for each cell, scaled by a representative of the flow rate. Typically, 1000 to 2000 iterations are needed to obtain a converged result, which takes about 1~2 hours on a 2.8 GHz Pentium 4 personal computer.

Numerical Procedure Validation and Uncertainty Estimate

The numerical procedure and methodology in this paper follow those in the studies of [22-23], in which the numerical results were qualified by comparing with the experimental data. In [23], the effect of various models on the computational results was examined, including the turbulence models, dispersed-phase modeling, different forces models, trajectory tracking model, near-wall grid arrangement, and mist injection scheme. In addition, the effects of flow inlet boundary conditions, inlet turbulence intensity, and the near-wall grid density on simulation results were also considered. The uncertainty from the key factors are estimated as: 10% for different turbulence models, 5% for turbulence length scales, 3% for resolution of second order central and upwind methods, 1% for convergence resolution, 3% for the effect of grid size, and 3% for the near-wall grid effect. The overall uncertainty for cooling effectiveness is estimated to be 12%. Since no experimental data in the public domain could be found to be compared with the current computational results under the simulated conditions. The above uncertainty is estimated from the computational results under low temperature and pressure conditions in [23]. Therefore, the estimated uncertainty is not centered with the true value, rather it represents the uncertainty excursion of the results that are attributed by the computational model and scheme.

RESULTS AND DISCUSSION

The gas turbine operating conditions selected in this study are featured by high temperature, high pressure, and high velocity of typical high-efficient commercial gas turbines, although not for any specific model. To study the mist enhancement on film cooling, an understanding on air-only film cooling is essential. Therefore, the results of air-only film cooling are discussed first in this section. In addition, the results of film cooling under low pressure, temperature and velocity are compared with the results at elevated gas turbine operating conditions.

Air Film Cooling at Gas Turbine Operating Conditions

Table 2 lists the physical parameters of nine cases studied for air-only film cooling at GT operating conditions. Note that Re_l is based on the airfoil chord length of 0.2 m, and Re_d is based on a jet diameter or slot width of 1.0 mm. Although the airfoil chord length is used as the length scale, the computational surface is flat. Figure 3 shows the adiabatic cooling effectiveness of the 2-D slot jet under different operating conditions. Compared to the result at low temperature, jet velocity and pressure (Case 2), the film cooling shows a very high cooling effectiveness at the elevated GT operating condition (Case 1). As shown in Table 1, when the pressure increases from 1 atm to 15 atm, the properties of specific heat capacity, thermal conductivity, and dynamic viscosity all increase except the kinematic viscosity decreases, which leads to a higher main flow and jet Reynolds numbers if the

chord length, jet size and velocity maintain the same. The extremely high cooling effectiveness can be interpreted by the change of these property values and the high Reynolds number.

Table 2 Studied cases of air-only film cooling without mist

	Type	T_{main} (K)	T_j (K)	u_{main} (m/s)	u_j (m/s)	P (atm)	M	Re_l $\times 10^{-6}$	Re_d $\times 10^{-3}$
1	Slot	1561	644	128	106	15	2	1.50	26.8
2	Slot	400	300	10	15	1	2	0.026	0.944
3	Simple Hole	1561	644	128	106	15	2	1.50	26.8
4	Simple Hole	1561	644	128	106	1	2	0.10	1.79
5	Fan-shaped	1561	644	128	106	15	2	1.50	26.8
6	Fan-shaped	400	300	10	15	1	2	0.026	0.944
7	Compound	1561	644	128	106	15	2	1.50	26.8
8	Compound	400	300	10	15	1	2	0.026	0.944
9	Simple Hole	1561	644	128	53	15	1	1.50	13.4

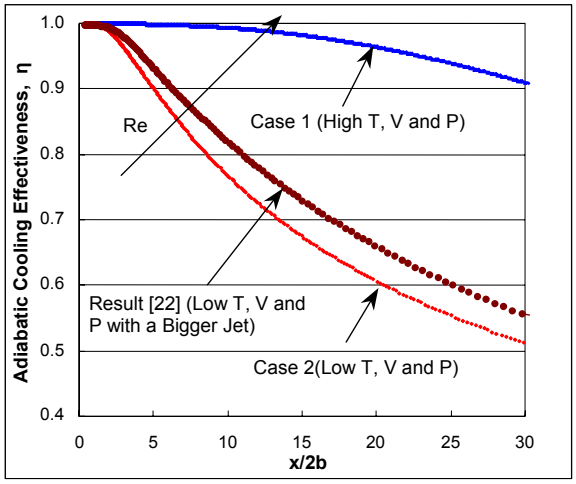

Figure 3 Comparison of slot jet adiabatic cooling effectiveness between low and elevated GT operating conditions

It is not clear exactly which change of physical property value plays a more important role than the changes of other property values. For simplicity, it can be seen that when Reynolds number increases, the adiabatic film cooling effectiveness (η) increases significantly. Case 1 seems to give an unrealistic high η, which does not prevail in 3-D cases (see Fig. 4). The reduced η may be caused by the secondary flow, which is absent from the 2-D cases. The secondary flow tends to wrap the hot air laterally from the sides to the bottom of the cooling jet flow, resulting to a reduced η distribution. Note the secondary flow here refers to the flow induced by the jet flow and perpendicular to the mainstream flow direction rather than the one caused by pressure gradient and geometric curvature in the through-flow passage.

The characteristics of the approaching boundary layer for 2-D cases with different operational conditions are documented in Table 3. The location is at 15 mm downstream of the mainstream inlet and 5 mm upstream of the coolant jet. Note that the boundary layer in the proximity of the coolant jet hole is affected by the jet flow and looses its characteristics of a undisturbed boundary layer.

Table 3 Characteristics of approaching boundary layers for 2-D cases with different operational conditions. The location is at 15 mm downstream the mainstream inlet and 5 mm before the coolant jet hole.

Case	δ (mm)	δ_1 (mm)	δ_2 (mm)	H_{12}	Re_δ	$Re_{\delta 1}$	$Re_{\delta 2}$
1	0.67	0.12	0.06	2.0	5360	960	480
2	0.81	0.34	0.11	3.0	307	129	42

Figure 4 shows the effect of elevated operating conditions on the simple round and fan-shaped cooling holes. For the simple round hole, the coolant jet flow detaches from the surface (not shown). The elevated operating conditions, with higher main flow Reynolds number, exacerbate the effect of secondary flow (Fig. 5) to scoop more hot gas and wrap it to the bottom of the cooling jet.

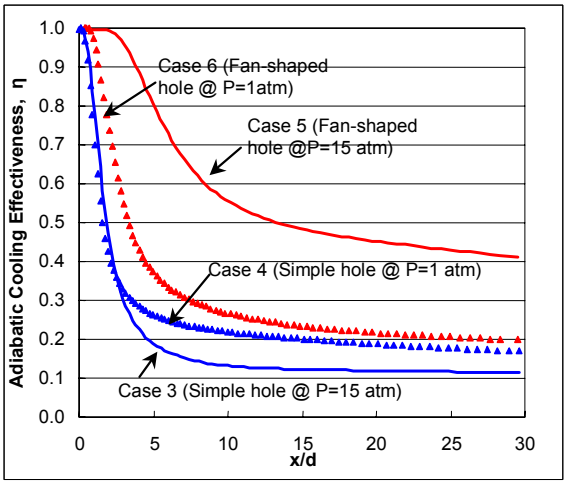

Figure 4 Effect of elevated operating conditions on adiabatic cooling effectiveness of 3-D film holes

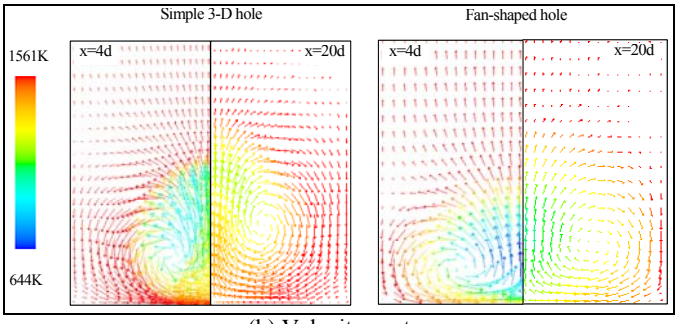

(b) Velocity vector

Figure 5 Cross-sectional velocity fields showing the secondary flow pattern (Film cooling without mist).

This 3-D secondary flow structure eventually degrades approximately 34% of the cooling performance of a simple round jet downstream of x/d=5. On the other hand, this does not happen to the fan-shaped hole, which typically produces strong diffusion and results to a wider surface cooling coverage. The lateral secondary flow downstream of a fan-shape hole is mild and limited to regime adjacent to the wall (see Fig. 5). Because of this fundamentally different

secondary flow behavior, under elevated operating conditions, the high main flow Reynolds number actually benefits the fan-shaped hole film cooling by pushing the coolant jet towards the surface without amplifying the downward wrapping of the degraded secondary flow. The significant increase of η is apparent immediately downstream of the injection hole and prevails as far as 30 jet diameters downstream with approximately a 100% increase of η value. The compound angle jet cases (Cases 7 and 8, not shown) share the similar results of the fan-shaped hole under elevated operating conditions.

A comprehensive study of the influences of different parameters on the film cooling effectiveness under low pressure and temperature conditions has been presented in [23]. For elevated gas turbine conditions, selected parameters are examined in this paper, including the blowing ratio, FSTI (free-stream turbulence intensity), and inlet velocity boundary layer.

Effect of Blowing Ratio – Figure 6 shows the effect of blowing ratio on a simple hole air film cooling. A blowing ratio of 2 is recommended in industrial application. By reducing the blowing ratio from 2 to 1 (using half of the previous cooling air, Case 9 vs. Case 3), the cooling effectiveness increases significantly. This could be explained as follows. Reducing the blowing ratio reduces the strength of the detached coolant jet flow. Correspondingly, the lateral wrapping motion of the secondary flow is reduced. In summary, under elevated GT operating conditions, blowing ratio is recommended be reduced to minimize separation of coolant jet from the surface because the adverse effect of the secondary flow will be amplified under elevated GT operating conditions. This would explain the degraded η values of Case 3. In Case 4 with a strong blowing ratio of 2, the coolant jet lifts off and separates from the surface along with a strong secondary flow structure. When the pressure is increased to 15 atm from Case 4 to Case 3, the lateral wrapping effect of the secondary flow is amplified by the increased main flow Reynolds number and results to a reduced cooling performance. Note that the effect of blowing ratio can be different for other injection holes.

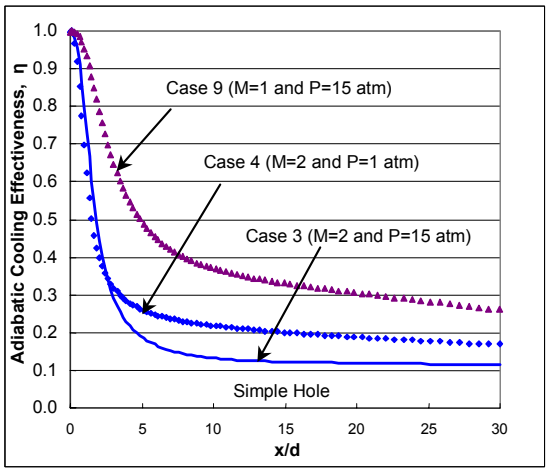

Figure 6 Effect of blowing ratio on a simple round hole adiabatic cooling effectiveness at elevated operating conditions

Effect of Inlet Turbulence Intensity – The turbulence intensity is assigned to 1% for the baseline case. In the actual operational conditions, the freestream turbulence intensity (FSTI) is usually higher. Figure 7 shows the effect of different inlet turbulence intensities at 5% and 10% respectively on adiabatic cooling effectiveness. For the simple round hole, higher FSTI results in a higher cooling effectiveness, which is due to the stronger mixing between the coolant flow and the flow close to the wall. However, the effect of FSTI for the 2-D slot-jet hole film cooling (not shown) is opposite: the higher FSTI results in a lower cooling effectiveness. This finding is consistent with the explanation in [6] and [23] under low pressure and temperature condition. Since the higher FSTI could either increase or decrease the film cooling effectiveness, a precise interpretation of the results is not attempted here. Nevertheless, built on the reasoning proposed by Mayhew et al. [6] plus the observations from this paper, the effect of FSTI could be qualitatively explained below: At higher blowing ratio (e.g. above 2), since the jet lifts off further from the surface, higher turbulence intensity helps bring the coolant back towards the wall and improve the film protection function; whereas at lower blowing ratio (e.g. 1), the film layer is close to the surface anyway, higher turbulence intensity tends to increase the mixing between the main flow and the wall, so subsequently reduces the film cooling effectiveness. There is not sufficient information to determine the demarcation value between high or low blowing ratio. The behavior of cooling jet and its interaction with the main flow is hypothesized as the governing factor that affects the influence of turbulence intensity.

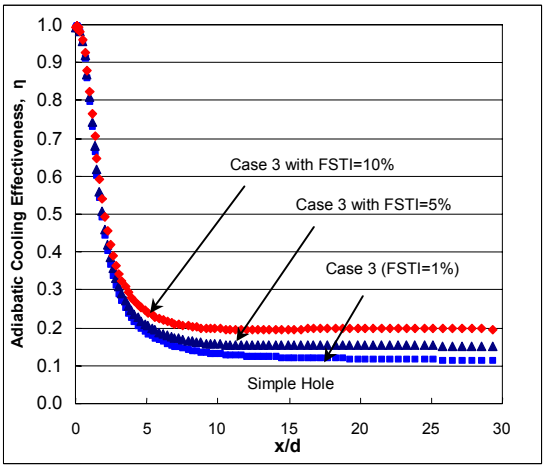

Figure 7 Effect of FSTI on a simple round hole adiabatic cooling effectiveness at 15 atm and 1561K.

Effect of Inlet Boundary Layer – In real applications, the characteristics of approaching boundary layer are another factor that could affect the film cooling results. Different velocity profiles, based on Blasius flows with a developing length of 5 mm and 10 mm, are applied at mainstream inlet to investigate its effect on film cooling. The results show that its effect on cooling effectiveness is negligible because the velocity is high in the current study, and the boundary layer thickness is found very thin (less than 0.7 mm).

Mist/Air Film Cooling at Gas Turbine Operating Conditions

The parametric values of mist/air film cooling cases are provided in Table 4. All the mist cooling cases are conducted at 15 atm, 1561 K of main flow temperature, 644K of coolant temperature, 128 m/s of main flow velocity, and 106 m/s of coolant jet velocity with 10% mist concentration and 10-μm water droplets. The mist concentration is the mass ratio of the water droplets to the coolant airflow rate. A 10% mist concentration requires approximately 0.3% of the main (or primary) mass flow rate in the real gas applications.

Table 4 Studied cases of mist/air film cooling using 10μm water droplets and 10% mist concentration at 15 atm and 1561 K.

	Type	T_j (K)	u_{main} (m/s)	u_j (m/s)	M	Re_{main} $\times 10^{-6}$	Re_{jet} $\times 10^{-3}$
10	Simple Hole	644	128	106	2	1.50	26.8
11	Fan-shaped	644	128	106	2	1.50	26.8
12	Compound	644	128	106	2	1.50	26.8

Figure 8 shows the temperature distribution as well as the droplet trajectories for both simple hole and compound-angle hole cases. The stochastic tracking method is employed to account for the turbulent dispersion, which can bring some of the droplets towards the wall and thus improves cooling.

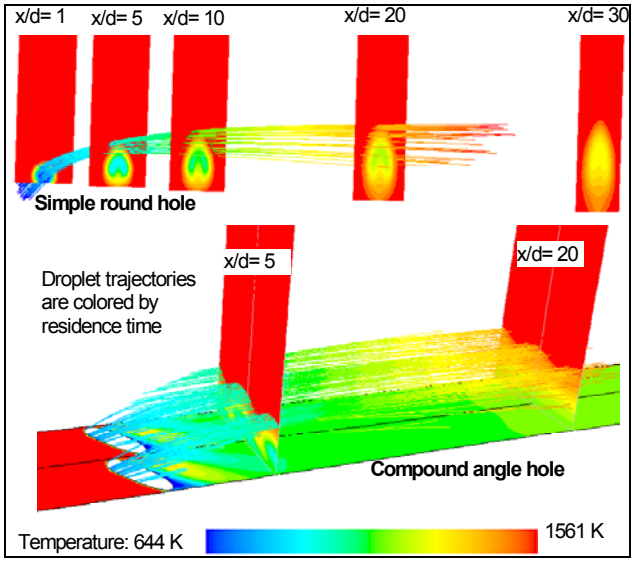

(a) Water droplet trajectories of simple and compound angle holes at 15 atm and 1561K. Droplets move away from the wall and the coolant flow and are shown on top of the coolant-affected area, so mist does not effectively enhance η under the elevated operating conditions.

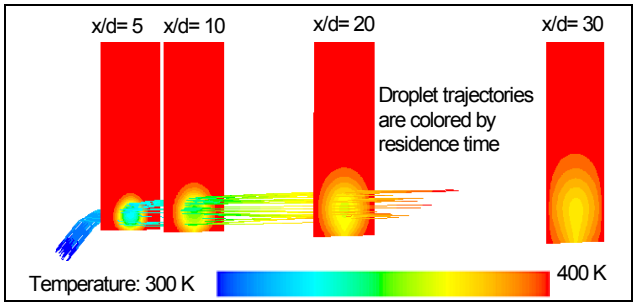

(b) Simple hole at low T, V and P conditions [22]

Figure 8 Comparison of water droplets trajectories and temperature field for simple and compound angle holes between low and elevated operating conditions. The coolant flow is not shown but the coolant-affected area can be recognized by the temperature field.

Different from the results of [22] at low temperature and velocity conditions (as seen in Fig. 8b), the droplets under elevated GT conditions (Fig. 8a) do not follow the streamline well due to the relatively high droplet momentum. Figure 8a shows the jet of a single round hole detaches from the wall, while the coolant jet of compound-angle hole stays to the surface and covers the adiabatic wall well. However, in both of these two cases, the droplets move away farther from the wall and the coolant flow. The coolant flow is not shown in Fig. 8, but the coolant flow field can be recognized by looking the temperature field. It can be seen that the water droplet trajectories under elevated operational conditions in Fig. 8a, are on top of the coolant-affected area, whereas in Fig. 8b, the water droplet trajectories coincide with the coolant affected area. Because of this droplet behavior, the mist does not effectively enhance η under the elevated operating conditions.

To be more realistic, only 3-D holes are considered for mist cooling cases. Figure 9 shows the adiabatic cooling effectiveness (η) with and without mist under elevated operating conditions. Consistent with the discussion above, the cooling enhancement is not as significant as under lower temperature and pressure conditions, in which the mist enhancement ranges from 40% to 50% downstream after x/d=15. As shown in Fig. 9, there is almost no enhancement for the simple-hole cases. The enhancement for the fan-shape hole cases is also negligible, so it is not shown in the figure. As to the compound angle hole cases, the enhancement increases roughly with x/d, and the maximum enhancement is about 7% at x/d=30. Note that there is a very small region close to x/d=0 where η_{mist}/η_0 is less than 1. This could be contributed by the computational uncertainty (less than 1%) between the two-phase mist/air calculation and the single air phase calculation near the hole region. The distribution of mist effect in the spanwise direction is shown in Fig. 10 for the compound angle hole (Case 12) at different distances from the injection hole. The cooling enhancement, approximately 7~8 percentage point, can be seen in the downstream after x/d=10 and prevails at all the locations in the spanwise direction (z).

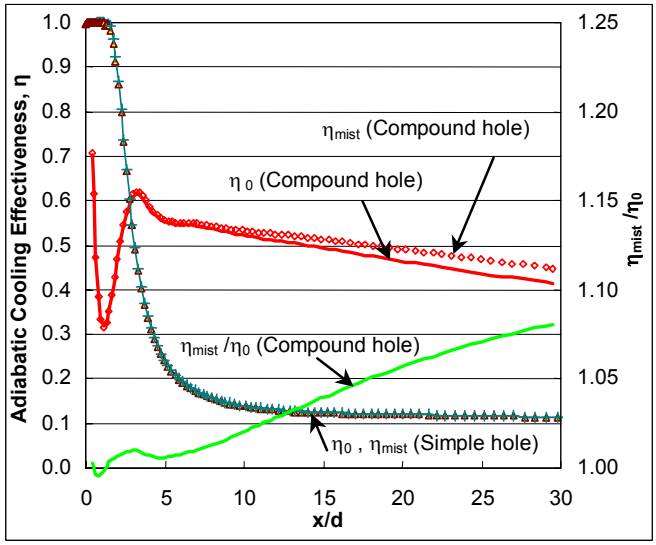

Figure 9 Enhancement of mist on film cooling along the centerline under the gas turbine operating conditions

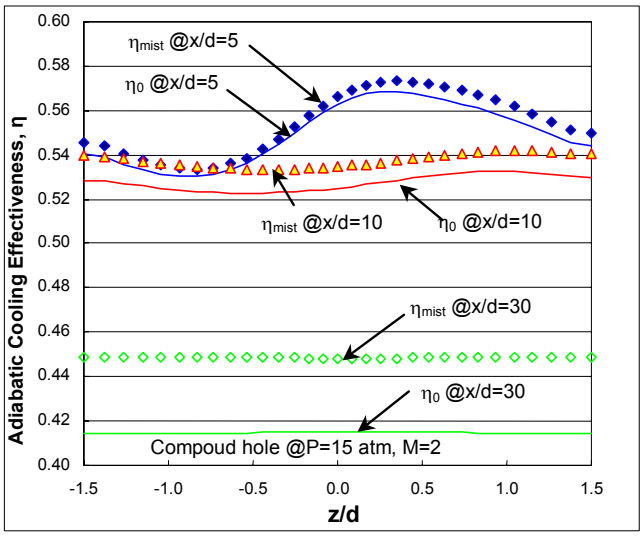

Figure 10 Distribution of adiabatic cooling effectiveness in spanwise direction (Compound angle hole, Case 12)

The effects of droplet size and mist concentration are studied with both fan-shaped and compound angle holes. The conditions of additional five cases are listed in Table 5. To evaluate how the droplet wall boundary conditions affect the mist cooling simulation, the "trap" condition, as an extreme case, is also tested. Note that the "trap" condition means that the droplet will adhere to the wall and evaporate completely once it hits the wall.

Table 5 Parametric values for studying effects of droplet size and mist concentration on mist film cooling

	Type	T_{main} (K)	T_j (K)	u_{main} (m/s)	u_j (m/s)	P (atm)	d (μm)	m (%)
13	Compound	1561	644	128	106	15	5	10
14	Compound	1561	644	128	106	15	20	10
15	Fan-shaped	1561	644	128	53	15	0	0
16	Fan-shaped	1561	644	128	53	15	10	10
17	Fan-shaped	1561	644	128	53	15	10	20

Effect of Droplet Size -- Comparison of the results of three droplet sizes (5, 10, and 20 μm) is shown in Fig. 11. Similar to the results under low pressure and temperature conditions [22-23], the smaller droplets are shown to provide better enhancements. There are two plausible explanations. Firstly, the small droplets provide higher surface to volume ratio, so evaporation completes more rapidly and effectively than the larger droplets. For film cooling, it is further advantageous to complete evaporation adjacent to the wall. Figure 8 shows that the droplets move away from the wall under elevated GT operating conditions. Therefore, it is plausible that the large droplets move farther away from the wall than small droplets under GT operating condition due to the high inertia force from jet injection. The second mechanism further contributes to ineffectiveness of producing film-cooling protection of the surface even though the latent heat absorption can reduce the main flow bulk temperature.

In the previous study under low pressure and temperature conditions [22-23], larger droplets may exit the computational domain without complete evaporation due to low evaporation rate or short residential time. However, under the GT operating conditions in the current study, all the droplets evaporate before x/d=30 (see Fig. 8) due to high main flow temperature and large temperature difference (917K) between the coolant and main flow. Since the jet flow seems to possess sufficient capacity to receive more mist flow, it is interesting to see the effect of injecting more mist into the jet flow.

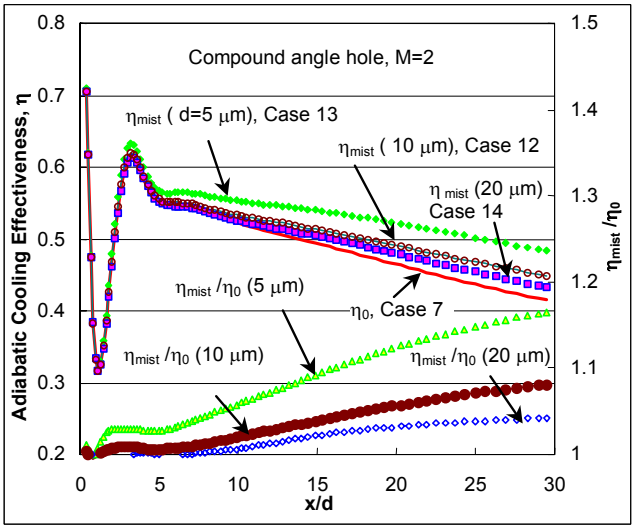

Figure 11 Effect of droplet size on mist cooling effectiveness (along the centerline of compound-angle hole cases 12 ~14)

Effect of Mist Concentration --- Figure 12 shows the results with different mist concentrations for the fan-shaped hole case. Since there is almost no enhancement for Case 11 with a blowing ratio of 2, a small blowing ratio of M=1 is used to examine the effect of mist concentration. It can be seen that the enhancement occurs at smaller blowing ratio. Furthermore, higher mist concentration results in a higher effectiveness for film cooling. When the mist concentration increases from 10% to 20%, the enhancement increases from 11% to 21% at x/d=30.

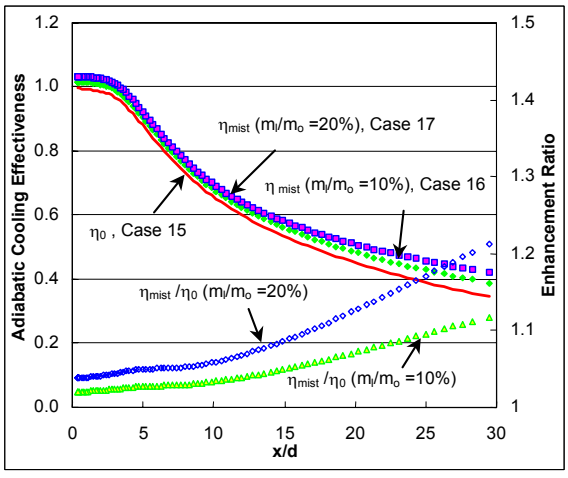

Figure 12 Effect of mist concentration on adiabatic cooling effectiveness (along the centerline of the fan-shaped hole cases 15, 16, and 17 with the blowing ratio M=1)

Effect of Droplet Boundary Conditions on the Wall – The model of "reflect" boundary conditions for the droplets on the wall may underestimate the mist cooling effectiveness because the important mechanism of droplet-wall interaction is not included. Li. et al. [34] analytically showed that the brief contact between the droplet and the wall plays a major role in transferring heat. Rather than correctly model the droplet-wall interactions, the "trap" wall condition is applied for comparison. With the "trap" droplet wall condition, the water droplets stick to the wall and evaporate. All the latent heat of droplets will be immediately released to the airflow. The true condition shall fall within these two extreme conditions. The results (not shown) indicate that no apparent difference is observed between the "reflect" and the "trap" conditions in the currently studied cases. This is because only very limited droplets (less than 1%) have a chance to hit the wall at GT operational conditions in this study. In other applications, such as jet impingement cooling, the results of the above two different boundary conditions are expected to be different.

Results Assessments

Although the cooling enhancements under elevated GT operating conditions are not as attractive as under low pressure and temperature conditions studied in [22-23], it is important to point out that in addition to the adiabatic film cooling effectiveness (η) the actual wall temperature reduction is another important indicator to evaluate the film cooling performance. The importance of evaluating the actual wall temperature reduction originates from the need to veer the wall temperature away from the blade material yield limit. An additional 50K wall temperature reduction will be appreciably valued when the wall temperature is close to the material yield point.

Under the elevated GT operating conditions, the temperature difference between main flow and coolant is approximately 917K (1561K-644K), whereas this temperature difference is 100K (400K-300K) under the low temperature and pressure conditions. Therefore, a 30K wall temperature reduction will contribute to 30 percentage points of η value under low pressure and temperature conditions, whereas the same 30K wall temperature reduction will only harness 3.3 percentage of η enhancement under elevated GT operating conditions. In other words, the same value of cooling enhancement should be evaluated differently under different operating conditions when the absolute surface temperature reduction is important.

Figure 13 shows the temperature distribution with and without mist along the centerline in the spanwise direction for the compound angle hole case. The maximum temperature reduction is 30K in this case. When the blowing ratio is reduced to 1 and the mist concentration increases to 20% as shown in Fig. 12, a meaningful wall cooling of additional 70K is achieved, which is based on an increase of 0.075 in cooling effectiveness and a temperature difference of 917 K (1561K- 644K) between the main flow and the coolant.

The objective of this study is to explore the performance of mist film cooling at real gas turbine operating conditions. The numerical simulation only provides a qualitative description of the trend and effects of various parameters. Experiments are needed to verify these results. The major reservation of applying mist film cooling from gas turbine OEMs and users is the concern related to erosion and corrosion of water droplets on the heated surface. The authors feel the corrosion issue should be negligible because the injected water mass is small. As stated earlier, the mass of a 10% mist concentration (based on the coolant mass flow rate) is approximately 0.3% of the main airflow rate. This amount is less than 1/3 of the moisture increase from the humidity change from 30% to 90% at 25°C ambient temperature. The erosion issue is also negligible, since all the droplets will evaporate quickly under the GT operating condition as shown in Fig. 8.

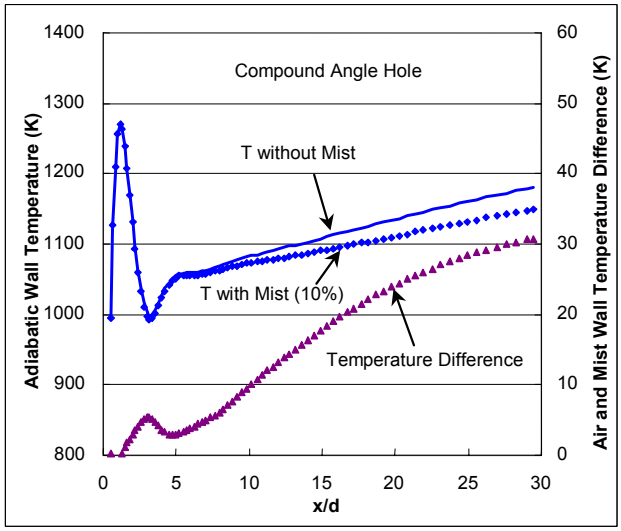

Figure 13 Adiabatic wall temperature distribution and reduction along the central line of compound-angle hole Case 12.

CONCLUSIONS

As a continuous effort to develop an advanced film-cooling scheme, this paper focuses on simulating mist film cooling under realistic gas turbine operating conditions at high temperature, velocity, pressure, and Reynolds number. The conclusions are:

- Droplets trajectories show that water droplets tend to move further away from the wall under GT operating conditions than under the low pressure and temperature conditions. The cooling effectiveness is downgraded due to this outward droplets excursion.
- The mist enhancement is less attractive in this study than found at low pressure and temperature cases in the previous studies. With a mist concentration of 10%, the maximum enhancement of adiabatic film cooling effectiveness is about 7% for the compound angle hole, corresponding to an additional adiabatic wall temperature reduction of 30K.
- Higher mist concentration will increase the cooling enhancement. When the mist concentration increases from 10% to 20%, the enhancement increases from 11% to 21% at x/d=30 for fan-shaped hole with a blowing ratio of 1. The adiabatic wall temperature reduces 70 K at x/d =30.
- Smaller droplets (5 μm) provide 10-20% better cooling performance than 10-μm droplets.
- Due to a large temperature difference between the main flow and the coolant flow under GT operating conditions, evaluation of the adiabatic film cooling effectiveness should be accompanied with the actual wall temperature reduction.

ACKNOWLEDGEMENT

This study is supported by the Louisiana Governor's Energy Initiative via the Clean Power and Energy Research Consortium (CPERC) and administered by the Louisiana Board of Regents.

REFERENCES

[1] Jia, R., Sunden, B., Miron, P., and Leger, B., 2003, "Numerical and Experimental Study of the Slot Film Cooling Jet with Various Angles," Proceedings of the ASME Summer Heat Transfer Conference, pp. 845-856.

[2] Bell, C. M., Hamakawa1, H., and Ligrani, P. M., 2000, "Film Cooling From Shaped Holes," ASME J. Heat Transfer, **122,** pp. 224-232.

[3] Brittingham, R.A. and Leylek, J. H, 2002, "A Detailed Analysis of Film Cooling Physics: Part IV—Compound-Angle Injection with Shaped Holes," ASME J. Turbomachinery, **122,** pp. 133-145.

[4] Taslim, M.E, and Khanicheh, A., 2005, "Film Effectiveness Downstream of a Row of Compound Angle Film Holes," ASME J. Heat Transfer, **127**, pp. 434-439.

[5] Kwak, J. S. and Han, J. C., 2003, "Heat Transfer Coefficients and Film-Cooling Effectiveness on a Gas Turbine Blade Tip," ASME J. Heat Transfer, **125,** pp. 494-502.

[6] Mayhew, J. E., Baughn, J. W., and Byerley, A. R., 2004, " Adiabatic Effectiveness of Film Cooling with Compound Angle Holes-The Effect of Blowing Ratio and Freestream Turbulence," ASME J. Heat Transfer, **126**, pp. 501-502.

[7] Wang, T., Chintalapati, S., Bunker, R. S., and Lee, C. P., 2000, "Jet Mixing in a Slot," Experimental Thermal and Fluid Science, **22**, pp. 1-17.

[8] Adami, P., Martelli, F., Montomoli, F., and Saumweber, C., 2002, "Numerical Investigation of Internal Crossflow Film Cooling," ASME Turbo Expo 02, **3A**, pp. 51-63.

[9] Ekkad, Srinath V., Ou, Shichuan; Rivir, Richard B., 2004, "A Transient Infrared Thermography Method for Simultaneous Film Cooling Effectiveness and Heat Transfer Coefficient Measurements from a Single Test," J. of Turbomachinery, **126**, pp. 597-603.

[10] Kwak, Jae Su and Han, Je-Chin, 2003, "Heat transfer Coefficients and Film Cooling Effectiveness on the Squealer Tip of a Gas Turbine Blade," ASME J. Turbomachinery, **125**, pp. 648-657.

[11] Heidmann, J. D., Rigby, D. L. and Ameri, A. A., 2000, "A Three-Dimensional Coupled Internal/External Simulation of a Film-Cooled Turbine Vane," J. Turbomachinery, **122**, pp. 348-359.

[12] Tyagi, Mayank, and Acharya, Sumanta, 2003, "Large Eddy Simulation of Film Cooling Flow from an Inclined Cylindrical Jet," ASME J. Turbomachinery, **125**, n. 4, pp. 734-742.

[13] Martini,P., Schulz ,A. and Bauer, JH, 2005, "Film Cooling Effectiveness and Heat Transfer on the Trailing Edge Cut-Back of Gas Turbine Airfoils With Various Internal Cooling Designs," ASME Turbo Expo 2005, Nevada, USA, June 6-9.

[14] Ahn, J., Schobeiri, M. T., Han, J.-C. and Moon, H. K., 2005, "Film Cooling Effectiveness on the Leading Edge of a Rotating Film-Cooled Blade Using Pressure Sensitive Paint," ASME Turbo Expo 2005, Nevada, USA, June 6-9.

[15] Rutledge, J. L., Robertson, D., and Bogard, D. G., 2005, "Degradation of Film Cooling Performance on a Turbine Vane Suction Side Due to Surface Roughness," ASME Turbo Expo 2005, Nevada, USA, June 6-9.

[16] Chaker, M., Meher-Homji, C.B., and Mee, M., 2002, "Inlet Fogging of Gas Turbine Engines - Part A: Fog Droplet Thermodynamics, Heat Transfer and Practical Considerations," ASME Proceedings of Turbo Expo 2002*,* **4**, pp. 413-428.

[17] Petr, V., 2003, "Analysis of Wet Compression in GT's," Energy and the Environment - Proceedings of the International Conference on Energy and the Environment, **1**, pp. 489-494.

[18] Guo, T., Wang, T., and Gaddis, J. L., 2000, "Mist/Steam Cooling in a Heated Horizontal Tube, Part 1: Experimental System, Part 2: Results and Modeling," ASME J. Turbomachinery, **122**, pp. 360–374.

[19] Guo, T., Wang, T., and Gaddis, J.L., 2001, "Mist/Steam Cooling in a 180^{o} Tube Bend," ASME J. Heat Transfer, **122,** pp. 749-756.

[20] Li, X., Gaddis, J. L., and Wang, T., 2003, "Mist/Steam Cooling by a Row of Impinging Jets," Int. J. Heat Mass Transfer, **46**, pp. 2279-2290.

[21] Li, X, Gaddis, J. L., and Wang, T, 2003, "Mist/Steam Heat Transfer with Jet Impingement onto a Concave Surface," ASME J. Heat Transfer, **125**, pp. 438-446

[22] Li, X. and Wang, T., 2005, "Simulation of Film Cooling Enhancement with Mist Injection," Accepted for publication in ASME Journal of Heat Transfer, also in Proc. ASME Turbo Expo 2005 (GT2005-69100), Reno, Nevada, June 6-9, 2005

[23] Li, X, and Wang, T, 2005, "Effects of Various Modeling on Mist Film Cooling," Proc. ASME Int. Mechanical Engineering Congress and Exhibition (IMECE 2005-81780), Orlando, Florida, November 2005.

[24] Wang, M. J. and Mayinger, F., 1995, "Post-dryout Dispersed Flow in Circular Bends," Int. J. Multiphase Flow, **21**, pp. 437-454.

[25] Aggarwal, S.K. and Park, T.W., 1999, "Dispersion of Evaporating Droplets in a Swirling Axisymmetric Jet," AIAA Journal, **37**, n. 12, pp. 1578-1587.

[26] Chen, X.-Q. and Pereira, J.C.F., 1995, "Prediction of Evaporating Spray in Anisotropically Turbulent Gas Flow," Numerical Heat Transfer; Part A: Applications, **27**, n. 2, pp. 143-162.

[27] Launder, B. E. and Spalding, D. B., 1972, Lectures in Mathematical Models of Turbulence*,* Academic Press, London, England.

[28] Wolfstein, M., 1969, "The Velocity and Temperature Distribution of One-Dimensional Flow with Turbulence Augmentation and Pressure Gradient," Int. J. Heat Mass Transfer, **12,** pp. 301-318.

[29] Ranz, W. E. and Marshall, W. R. Jr., 1952, "Evaporation from Drops, Part I," Chem. Eng. Prog., **48**, pp. 141-146.

[30] Ranz, W. E. and Marshall, W. R. Jr., 1952, "Evaporation from Drops, Part II," Chem. Eng. Prog., **48**, pp. 173-180.

[31] Kuo, K. Y., 1986*,* Principles of Combustion, John Wiley and Sons, New York.

[32] Fluent Manual, Version 6.2.16, 2005, Fluent, Inc.

[33] Wang, T., Li, X., and Pinninti, V., 2004, "Simulation of Mist Transport for Gas Turbine Inlet Air Cooling," Proceedings of ASME International Mechanical Engineering Congress & Exposition, Anaheim, California.

[34] Li, X., Gaddis, J. L., and Wang, T., 2001, "Modeling of Heat Transfer in a Mist/Steam Impingement Jet," ASME J. Heat Transfer, **123**, pp. 1086-1092